Inorg. Chem. **2004**, *43*, 2105–2113

Iron(II) Carboxylate Complexes Based on a Tetraimidazole Ligand as Models of the Photosynthetic Non-Heme Ferrous Sites: Synthesis, Crystal Structure, and Mössbauer and Magnetic Studies

Gilles Lemercier,[†,‡] Etienne Mulliez,[§] Chantal Brouca-Cabarrecq,[†,||] Françoise Dahan,[†] and Jean-Pierre Tuchagues*[,†]

Laboratoire de Chimie de Coordination, UPR CNRS 8241, 205 route de Narbonne, 31077 Toulouse Cédex 4, France, and Laboratoire de Chimie et Biochimie des Centres Rédox Biologiques, DBMS, CEA/CNRS/Université Joseph Fourier, 17 Avenue des Martyrs, 38054 Grenoble Cedex 09, France

Received July 31, 2003

The preparations, X-ray structures, and detailed physical characterization are presented for new complexes involving an iron(II) center, a tetraimidazole ligand (TIM), and different carboxylates. $[Fe(TIM)(C_6H_5CH_2CO_2)](ClO_4)$ (**1**) crystallizes in the *Pbca* space group with $a = 10.8947(13)$, $b = 20.343(2)$, and $c = 22.833(3)$ Å, $Z = 8$, and $V = 5060.6(11)$ Å^3. $[Fe(TIM)(CH_3CO_2)](ClO_4)$ (**2**) crystallizes in the *Ia* space group with $a = 17.117(2)$, $b = 10.3358(12)$, and $c = 25.658(3)$ Å, $\beta = 90.301(13)°$, $Z = 8$, and $V = 4539.5(9)$ Å^3. In both structures, the iron(II) is hexacoordinated to the four $N_{imidazole}$ donors of the TIM ligand and the two O donors of a bidentate carboxylate. The flexibility of the carboxylate bidentate coordination, symmetrical or more or less asymmetrical, associated with the steric demand of the TIM ligand results in a remarkable versatility of the $Fe^{II}N_4O_2$ coordination geometry. The diversity in carboxylate bidentate coordination modes has allowed us to clearly show the importance of the structural and electronic effects, through IR and Mössbauer spectroscopy, of this apparently tenuous carboxylate shift. Comparison of the structural and Mössbauer properties of these complexes with the non-heme ferrous site of photosynthetic systems (i) shows that the metric parameters of site **2b**, including the symmetrically chelated bidentate carboxylate, are closer to those of the non-heme ferrous site in the bacterial reaction centers of *Rhodopseudomonas viridis* and *R. sphaeroides* and (ii) suggests that the ligand environment of the non-heme ferrous center of PS 2 is close to the axially distorted octahedral symmetry resulting from an asymmetrical bidentate coordination of the $-CO_2$ motif, as in complex **1**.

Introduction

Non-heme iron metalloproteins with mono active sites are involved in various biological processes.[1] The X-ray crystal structure has been established for a number of such metalloproteins, including lipoxygenases,[2] Fe superoxide dismutase (SOD),[3] hemerythrin,[4] isopenicilin N-synthase (IPSN),[5] intra- and extradiol dioxygenases,[6] etc. A pyramidal coordination

* To whom correspondence should be addressed. E-mail: tuchague@lcc-toulouse.fr.

† Laboratoire de Chimie de Coordination.

‡ Present address: École Normale Supérieure de Lyon, Laboratoire de Chimie UMR CNRS and ENS-Lyon No. 5532, 46 allée d'Italie, 69364 Lyon Cédex 07, France. E-mail: gilles.lemercier@ens-lyon.fr.

§ Laboratoire de Chimie et Biochimie des Centres Rédox Biologiques.

|| Present address: Centre d'Elaboration de Matériaux et d'Etudes Structurales, UPR CNRS 8011, 29 rue Jeanne Marvig, 31055 Toulouse Cédex, France.

(1) (a) Solomon, E. I.; Brunold, T. C.; Davis, M. I.; Kemsley, J. N.; Lee, S. K.; Lehnert, N.; Neese, F.; Skulan, A. J.; Yang, Y. S.; Zhou, J. *Chem. Rev.* **2000**, *100*, 235. (b) Holm, R. H.; Kennepohl, P.; Solomon, E. I. *Chem. Rev.* **1996**, *96*, 2239. (c) Lippard, S. J.; Berg, J. M. *Principals of Bioinorganic Chemistry*; University Science Books: Mill Valley, CA 94941, 1994.

(2) (a) Minor, W.; Steckzko, J.; Stec, B.; Otwinowski, Z.; Bolin, J. T.; Walter, R.; Axelrod, B. *Biochemistry* **1996**, *35*, 10687. (b) Skrzypczak-Jankun, E.; Amzel, L. M.; Kroa, B. A.; Funk, M. O. J. *Proteins: Struct., Funct., Genet.* **1997**, *29*, 15.

(3) (a) Cooper, J. B.; Mclntyre, K.; Badasso, M. O.; Wood, S. P.; Zhang, Y.; Garbe, T. R.; Young, D. *J. Mol. Biol.* **1995**, *246*, 531. (b) Lah, M. S.; Dixon, M. M.; Pattridge, K. A.; Stallings, W. C.; Fee, J. A.; Ludwig, M. L. *Biochemistry* **1995**, *34*, 1646. (c) Ringe, D.; Petsko, G. A.; Yamakura, K.; Suzuki, D.; Ohmori, D. *Proc. Natl. Acad. Sci. U.S.A.* **1983**, *80*, 3879. (d) Stallings, W. C.; Powers, T. B.; Pattridge, K. A.; Fee, J. A.; Ludwig, M. L. *Proc. Natl. Acad. Sci. U.S.A.* **1983**, *80*, 3884. (e) Sttoddard, B. L.; Howell, P. L.; Ringe, D.; Petsko, G. A. *Biochemistry* **1995**, *29*, 8885.

(4) (a) Pulver, S.; Froland, W. A.; Fox, B. G.; Lipscomb, J. D.; Solomon, E. I. *J. Am. Chem. Soc.* **1993**, *115*, 12049. (b) Reem, R. C.; McCormick, J. C.; Richardson, D. E.; Devin, F. J.; Stephens, P. J.; Musselman, R. L.; Solomon, E. I. *J. Am. Chem. Soc.* **1989**, *111*, 8. (c) Stenkamp, R. E. *Chem. Rev.* **1994**, *94*, 715.

10.1021/ic034907k CCC: $27.50
Published on Web 02/18/2004

arrangement of three histidyl nitrogen donors is often found at the metal sites of such proteins. A quite different coordination structure characterizes the non-heme iron located between the primary and secondary quinone electron acceptors of the reaction centers in photosynthetic bacteria[7] and photosystem 2 of oxygenic photosynthetic organisms.[8] The X-ray structure determination of the reaction centers of two different photosynthetic bacteria, *Rhodopseudomonas viridis*[9] and *R. sphaeroides*,[10] indicates that the ferrous ion is in a distorted-octahedral ligand environment including four nitrogen atoms pertaining to the imidazole moiety of histidine residues and two oxygen atoms from a glutamic acid residue of the surrounding protein.

A few iron(II) complexes including imidazole ligands have been previously reported.[11] However, none of them possess the unique structural characteristics of the non-heme ferrous iron of photosynthetic systems. Owing to the interest of ferrous complexes as models of the ferrous center of mononuclear non-heme iron-containing proteins, we have synthesized and studied a novel series of chelates resulting from the reaction of a tetraimidazole ligand, bis[(imidazol-4-methyl)-4′-imidazol-2′-yl]methane,[12] abbreviated TIM, with ferrous salts. In this report, we describe the synthesis and IR, Mössbauer, and variable-temperatue magnetic susceptibility results for $[Fe(TIM)(C_6H_5CH_2CO_2)](ClO_4)$ (**1**), $[Fe(TIM)(CH_3CO_2)](ClO_4)$ (**2**), $Fe_2(TIM)_2(C_2O_4)(ClO_4)_2$ (**3**), $Fe(TIM)(HCO_2)_2$ (**4**), and $Fe(TIM)(CH_3CO_2)_2$ (**5**). X-ray crystal structure determinations of **1** and **2** have also been performed.

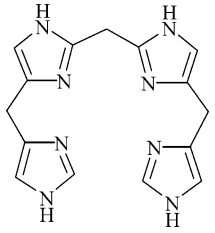

Figure 1. Schematic representation of bis[(imidazol-4-methyl)-4′-imidazol-2′-yl]methane (TIM).

Experimental Section

Materials. All reagents were of analytical grade and used without further purification. Solvents were degassed under vacuum prior to use. Ferrous acetate and ferrous formate were prepared according to the method of Schreurer−Kestner as modified by Rhoda et al.[13] Due to the high reactivity of iron(II) salts and complexes with dioxygen, all complexes were prepared under a purified nitrogen atmosphere in Schlenk-type vessels or in an inert-atmosphere box (Vacuum Atmosphere HE 43-2) equipped with a Dry-Train (Jahan EVAC 7).

Ligand. The tetraimidazole ligand TIM (Figure 1) was prepared as a faint-yellow microcrystalline powder, according to the described procedure.[12]

Complexes. In a typical reaction for the synthesis of complexes $[Fe(TIM)(C_6H_5CH_2CO_2)](ClO_4)$ (**1**), $[Fe(TIM)(CH_3CO_2)](ClO_4)$ (**2**), and $Fe_2(TIM)_2(C_2O_4)(ClO_4)_2$ (**3**), TIM·$2H_2O$ (0.6 mmol) was slowly added as a solid to a yellow-green solution of $Fe(ClO_4)_2$·$6H_2O$ (0.6 mmol) in methanol (7 mL) under stirring. The appropriate sodium carboxylate was then added to the purple-red reaction mixture (2.1 equiv of solid sodium phenylacetate for **1**, 1.3 equiv of a methanolic solution of sodium acetate (105 mg in 1 mL) for **2**, 0.55 equiv of an aqueous solution of sodium oxalate (33.5 mg in 5 mL) for **3**). Complexes **1**−**3** slowly precipitated out of the reaction mixture and were collected by filtration after 24 h (**1**, white-pale pink; **2**, white-light green; **3**, brown-orange). In the case of complex **3**, a strict control of the sodium oxalate ratio was needed to minimize simultaneous formation of the mononuclear species, $Fe(TIM)(C_2O_4Na)(ClO_4)$; on the other hand, attempts at preparing this mononuclear species as a pure compound by increasing the sodium oxalate ratio failed. $Fe(TIM)(HCO_2)_2$ (**4**) and $Fe(TIM)(CH_3CO_2)_2$ (**5**) were obtained by direct reaction of TIM·$2H_2O$ (1.37 mmol, as a solid) with a methanolic solution (7 mL) of $Fe(HCO_2)_2$·$2H_2O$ and $Fe(CH_3CO_2)_2$·$2H_2O$ (1.37 mmol), respectively. After 14 h of reaction, a small amount of precipitate was eliminated by filtration and 6−7 equiv (vol) of CH_3CN was added to the reaction mixture yielding a precipitate which was collected by filtration (**4**, pale yellow; **5**, white-green). Complexes **1**−**5** were finally dried under vacuum.

$[Fe(TIM)(C_6H_5CH_2CO_2)](ClO_4)$ (**1**): yield 160 mg (45%). Anal. Calcd for $FeC_{23}H_{23}N_8O_6Cl$: C, 46.1; H, 3.9; N, 18.7; Cl, 5.9; Fe, 9.3. Found: C, 46.1; H, 3.8; N, 19.0; Cl, 5.8; Fe, 9.2. $[Fe(TIM)CH_3CO_2](ClO_4)$ (**2**): yield 190 mg (30%). Anal. Calcd for $FeC_{18}H_{23}N_8O_7Cl$: C, 39.0; H, 4.2; N, 20.2; Cl, 6.4; Fe, 10.0. Found: C, 39.2; H, 3.8; N, 20.5; Cl, 7.1; Fe, 10.0. $Fe_2(TIM)_2(C_2O_4)(ClO_4)_2$ (**3**): yield 160 mg (85%). Anal. Calcd for $Fe_2C_{32}H_{32}N_{16}O_{12}Cl_2$: C, 37.8; H, 3.8; N, 21.9; Cl, 7.0; Fe, 11.0. Found: C, 37.9; H, 3.2; N, 21.8; Cl, 6.7; Fe, 11.3. $Fe(TIM)(HCO_2)_2$ (**4**): yield 300 mg (46%). Anal. Calcd for $FeC_{17}H_{18}N_8O_4$: C, 45.0; H, 4.0; N, 24.7; Fe, 12.3. Found: C, 45.3; H, 4.1; N, 25.2; Fe, 11.2. $Fe(TIM)(CH_3-$

(5) Roach, P. L.; Cliflon, I. J.; Hensgens, C. M. H.; Shibata, N.; Schofield, C. J.; Hajdu, J.; Baldwin, J. E. *Nature* **1997**, *387*, 827.

(6) (a) Ohlendorf, D. H.; Lipscomb, J. D.; Weber, P. C. *Nature (London)* **1988**, *336*, 403. (b) Ohlendorf, D. H.; Orville, A. M.; Lipscomb, J. D. *J. Mol. Biol.* **1994**, *244*, 586. (c) Kita, A.; Kita, S.; Fujisawa, I.; Inaka, K.; Ishida, T.; Horiike, K.; Nozaki, M.; Miki, K. *Structure* **1999**, *7*, 25. (d) Sugimoto, K.; Senda, T.; Aoshima, H.; Masai, E.; Fukuda, M.; Mitsui, Y. *Structure* **1999**, *7*, 953.

(7) Clayton, R. K., Sistrom, W. R., Eds. *The Photosynthetic Bacteria*; Plenum: New York, 1978.

(8) (a) Nugent, J. H. A.; Diner, B. A.; Evans, M. C. W. *FEBS Lett.* **1981**, *124*, 241. (b) Petrouleas, V.; Diner, B. A. *FEBS Lett.* **1982**, *147*, 111.(c) Petrouleas, V.; Diner, B. A. *Adv. Photosynth. Res., Proc. Int. Congr. Photosynth., 6th* **1984**, *1*, part 2, 195. (d) Rutherford, A. W.; Zimmerman, J. L. *Biochim. Biophys. Acta* **1984**, *767*, 168. (e) Diner, B. A.; Petrouleas, V. *Biochim. Biophys. Acta* **1986**, *849*, 264.

(9) (a) Deisenhofer, J.; Epp, O.; Miki, K.; Huber, R.; Michel, H. *J. Mol. Biol.* **1984**, *180*, 385. (b) Deisenhofer, J.; Epp, O.; Miki, K.; Huber, R.; Michel, H. *Nature* **1985**, *318*, 19. (c) Michel, H.; Epp, O.; Deisenhofer, J. *EMBO J.* **1986**, *5*, 2445.

(10) (a) Allen, J. P.; Feher, G.; Yeates, T. O.; Komiya, H.; Rees, D. C. *Proc. Natl. Sci. U.S.A.* **1988**, *85*, 8487. (b) Allen, J. P.; Feher, G.; Yeates, T. O.; Komiya, H.; Rees, D. C. *Proc. Natl. Sci. U.S.A.* **1987**, *84*, 5730.

(11) (a) Holmes, F.; Jones, K. M.; Torrible, E. G. *J. Chem. Soc.* **1961**, 4790. (b) Abushamleh, A. S.; Goodwin, H. A. *Aust. J. Chem.* **1979**, *32*, 513. (c) Guillot, G.; Mulliez, E.; Leduc, P.; Chottard, J. C. *Inorg. Chem.* **1990**, *29*, 577. (d) Boinnard, D.; Cassoux, P.; Petrouleas, V.; Savariault, J.-M.; Tuchagues, J.-P. *Inorg. Chem.* **1990**, *29*, 4114. (e) Martinez Lorente, M. A.; Petrouleas, V.; Savariault, J.-M.; Poinsot, R.; Drillon, M.; Tuchagues, J.-P. *Inorg. Chem.* **1991**, *30*, 3587. (f) Bois, C.; Bousseksou, A.; Nitsche, W.; Mulliez, E.; Guillot-edeheit, G.; Leduc, P.; Chottard, J.-C. *New J. Chem.* **1992**, *16*, 435. (g) Martinez Lorente, M. A.; Dahan, F.; Petrouleas, V.; Bousseksou, A.; Tuchagues, J.-P. *Inorg. Chem.* **1995**, *34*, 5346. (h) Bousseksou, A.; Verelst, M.; Constant-Machado, H.; Lemercier, G.; Tuchagues, J.-P.; Varret, F. *Inorg. Chem.* **1996**, *35*, 110.

(12) Mulliez, E. *Tetrahedron Lett.* **1989**, *30*, 6169.

(13) (a) Schreurer-Kestner, M. A. *Bull. Soc. Chim. Fr.* **1863**, *5*, 345. (b) Rhoda, R. N.; Fraioli, A. V. *Inorg. Synth.* **1953**, *4*, 159.

$CO_2)_2$ (**5**): yield 286 mg (84%). Anal. Calcd for $FeC_{20}H_{26}N_8O_4$: C, 46.7; H, 5.1; N, 21.8; Fe, 10.8. Found: C, 46.2; H, 4.7; N, 22.1; Fe, 10.4.

Single crystals of **1** and **2** suitable for X-ray diffraction studies were obtained by slow evaporation of the filtrate in the glovebox.

Caution! *Perchlorate salts of compounds containing organic ligands are potentially explosive. Although we have encountered no such problems with these complexes, only small quantities should be prepared and handled with care.*

Physical Measurements. Elemental analyses were carried out at the Laboratoire de Chimie de Coordination Microanalytical Laboratory in Toulouse, France, for C, H, and N and at the Service Central de Microanalyze du CNRS in Vernaison, France, for Cl and Fe.

IR spectra were recorded in the 200−4000 cm^{-1} range on a Perkin-Elmer 983 spectrophotometer coupled with a Perkin-Elmer infrared data station. Samples were run as CsBr pellets prepared under nitrogen in the glovebox.

Variable-temperature magnetic susceptibility measurements were obtained with a Quantum Design MPMS SQUID susceptometer as previously described.[14] All samples were 3 mm diameter pellets molded in the glovebox from microcrystalline samples. Magnetic susceptibility measurements were performed in the 2−300 K temperature range, and diamagnetic corrections were applied by using Pascal's constants. Least-squares computer fittings of the experimental data were accomplished with an adapted version of the function-minimization program STEPT.[15]

Mössbauer measurements were obtained on a constant-acceleration spectrometer with a 50 mCi source of ^{57}Co (Rh matrix). Isomer shift values (δ) are given with respect to metallic iron at room temperature. The absorber was a sample of 100 mg of microcrystalline powder enclosed in a 20 mm diameter cylindrical plastic sample holder, the size of which had been determined to optimize the absorption. Variable-temperature spectra were obtained in the 80−305 K range, by using a MD306 Oxford cryostat, the thermal scanning being monitored by an Oxford ITC4 servocontrol device (±0.1 K accuracy). A least-squares computer program[16] was used to fit the Mössbauer parameters and determine their standard deviations of statistical origin (given in parentheses).

Crystallographic Data Collection and Structure Determination. The selected crystals of **1** (translucid plate, 0.50 × 0.50 × 0.10 mm^3) and **2** (colorless parallelepiped, 0.40 × 0.35 × 0.30 mm^3) were coated with vaselin under an inert atmosphere and sealed in Lindemann glass capillaries and then mounted on an Enraf-Nonius CAD4 diffractometer using a graphite-monochromated Mo Kα radiation (λ = 0.710 73 Å). Data were collected at 293 K up to 27° for **1** and to 26° for **2** in the $\omega-2\theta$ scan mode and reduced with the MolEN package.[17] A total of 5493 reflections, all independent, were collected for **1**, and 6737 reflections, all independent, were collected for **2**. Absorption corrections[18] from ψ scans were applied ($T_{min-max}$ = 0.9210−0.9999 for **1**, $T_{min-max}$ = 0.9800−0.9971 for **2**). The structures were solved using SHELXS-97[19] and refined on F^2 by full-matrix least-squares using SHELXL-97[20] with anisotropic displacement parameters for all non-hydrogen atoms. H atoms were introduced in calculations using the riding model with isotropic U_H equal to 1.1 times that of the riding atom. In **1**, three oxygen atoms of the perchlorate anion were found disordered and refined in the 60/40 ratio. In **2**, four oxygen atoms of one ot the two perchlorate anions were found disordered and refined in the 60/40 ratio. The atomic scattering factors and anomalous dispersion terms were taken from the standard compilation.[21] The maximum and minimum peaks on the final difference Fourier map were 0.438 and −0.376 e A^{-3} for **1** and 0.210 and −0.208 e $Å^{-3}$ for **2**. Drawings of the molecules were performed with the program ZORTEP.[22] Crystal data collection and refinement parameters are given in Table 1, and selected bond distances and angles are gathered in Tables 2 and 3 for **1** and **2**, respectively.

Table 1. Crystallographic Data for [Fe(TIM)($C_6H_5CH_2CO_2$)](ClO_4) (**1**) and [Fe(TIM)(CH_3CO_2)](ClO_4) (**2**)

	1	**2**
chem formula	$C_{23}H_{23}ClFeN_8O_6$	$C_{17}H_{19}ClFeN_8O_6$
fw	598.79	522.7
space group	*Pbca* (No. 61)	*Ia* (No. 9)
a, Å	10.8947(13)	17.117(2)
b, Å	20.343(2)	10.3358(12)
c, Å	22.833(3)	25.658(3)
β, deg		90.301(13)
V, $Å^3$	5060.6(11)	4539.5(9)
Z	8	8
ρ_{calcd}, $g\cdot cm^{-3}$	1.572	1.530
γ, Å	0.710 73	0.710 73
T, K	293(2)	293(2)
μ(Mo Kα), cm^{-1}	7.59	5.80
R^a (obsd, all)	0.0383, 0.0431	0.0259, 0.0404
$R_w{}^b$ (obsd, all)	0.0927, 0.0931	0.0585, 0.0632

^{a} $R = \sum||F_o| - |F_c||/\sum|F_o|$. ^{b} $R_w = [\sum w(|F_o|^2 - |F_c|^2)^2/\sum w|F_o^2|^2]^{1/2}$.

Table 2. Selected Interatomic Distances (Å) and Angles (deg) for [Fe(TIM)($C_6H_5CH_2CO_2$)](ClO_4) (**1**)

Fe−N(1)	2.1762(18)	Fe−N(3)	2.1367(18)
Fe−N(2)	2.1023(17)	Fe−N(4)	2.1064(19)
Fe−O(1)	2.1634(16)	Fe−O(2)	2.3259(16)
N(1)−Fe−N(2)	86.21(7)	N(2)−Fe−O(1)	145.55(6)
N(1)−Fe−N(3)	168.63(7)	N(2)−Fe−O(2)	87.66(6)
N(1)−Fe−N(4)	94.28(7)	N(3)−Fe−N(4)	84.44(7)
N(1)−Fe−O(1)	91.58(7)	N(3)−Fe−O(1)	99.79(7)
N(1)−Fe−O(2)	89.26(6)	N(3)−Fe−O(2)	96.58(6)
N(2)−Fe−N(3)	84.29(7)	N(4)−Fe−O(1)	97.81(7)
N(2)−Fe−N(4)	116.64(7)	N(4)−Fe−O(2)	155.59(6)
O(1)−Fe−O(2)	57.91(6)		

Results and Discussion

Syntheses. Reaction of the acyclic neutral tetraimidazole ligand TIM with ferrous acetate and ferrous formate yielded complexes analyzing for one TIM ligand and two carboxylates per iron. These complexes are soluble in alcohols, and addition of acetonitrile was required to separate them from the reaction medium as faintly colored microcrystalline

(14) Clemente-Juan, J. M.; Mackiewicz, C.; Verelst, M.; Dahan, F.; Bousseksou, A.; Sanakis, Y.; Tuchagues, J.-P. *Inorg. Chem.* **2002**, *41*, 1478.
(15) Chandler, J. P. *Quantum Chemistry Program Exchange*; Indiana University: Bloomington, IN, 1973; Program 66.
(16) Varret, F. *Proceedings of the International Conference on Mössbauer Effect Applications*, Jaipur, India, 1981; Indian National Science Academy: New Delhi, 1982.
(17) Fair, C. K. *MolEN. Structure Solution Procedures*; Enraf-Nonius: Delft, Holland, 1990.
(18) North, A. C. T.; Phillips, D. C.; Mathews, F. S. *Acta Crystallogr., Sect. A* **1968**, *A24*, 351.
(19) Sheldrick, G. M. *SHELXS-97. Program for Crystal Structure Solution*; University of Göttingen: Göttingen, Germany, 1990.
(20) Sheldrick, G. M. *SHELXL-97. Program for the refinement of crystal structures from diffraction data*; University of Göttingen: Göttingen, Germany, 1997.
(21) *International Tables for Crystallography*; Kluwer Academic Publishers: Dordrecht, The Netherlands, 1992; Vol. C, Tables 4.2.6.8 and 6.1.1.4.
(22) Zsolnai, L.; Pritzkow, H.; Huttner, G. *ZORTEP. Ortep for PC, Program for Molecular Graphics*; University of Heidelberg: Heidelberg, Germany, 1996.

Table 3. Selected Interatomic Distances (Å) and Angles (deg) for [Fe(TIM)(CH_3CO_2)](ClO_4) (**2**)

Fe(1)−N(1a)	2.166(3)	Fe(2)−N(1b)	2.112(3)
Fe(1)−N(3a)	2.112(2)	Fe(2)−N(3b)	2.192(3)
Fe(1)−N(5a)	2.148(3)	Fe(2)−N(5b)	2.126(2)
Fe(1)−N(7a)	2.119(3)	Fe(2)−N(7b)	2.217(3)
Fe(1)−O(1a)	2.108(2)	Fe(2)−O(1b)	2.227(2)
Fe(1)−O(2a)	2.435(3)	Fe(2)−O(2b)	2.263(2)
N(1a)−Fe(1)−N(3a)	86.59(10)	N(1b)−Fe(2)−N(3b)	85.20(10)
N(1a)−Fe(1)−N(5a)	170.16(11)	N(1b)−Fe(2)−N(5b)	114.00(11)
N(1a)−Fe(1)−N(7a)	98.67(10)	N(1b)−Fe(2)−N(7b)	91.56(10)
N(1a)−Fe(1)−O(1a)	92.43(10)	N(1b)−Fe(2)−O(1b)	157.51(9)
N(1a)−Fe(1)−O(2a)	91.51(9)	N(1b)−Fe(2)−O(2b)	99.65(10)
N(3a)−Fe(1)−N(5a)	83.80(10)	N(3b)−Fe(2)−N(5b)	83.45(10)
N(3a)−Fe(1)−N(7a)	116.33(10)	N(3b)−Fe(2)−N(7b)	166.49(10)
N(3a)−Fe(1)−O(1a)	97.14(9)	N(3b)−Fe(2)−O(1b)	100.48(9)
N(3a)−Fe(1)−O(2a)	153.05(9)	N(3b)−Fe(2)−O(2b)	104.12(10)
N(5a)−Fe(1)−N(7a)	83.79(10)	N(5b)−Fe(2)−N(7b)	85.91(10)
N(5a)−Fe(1)−O(1a)	90.84(10)	N(5b)−Fe(2)−O(1b)	88.37(9)
N(5a)−Fe(1)−O(2a)	98.00(9)	N(5b)−Fe(2)−O(2b)	146.11(10)
N(7a)−Fe(1)−O(1a)	145.15(9)	N(7b)−Fe(2)−O(1b)	87.50(9)
N(7a)−Fe(1)−O(2a)	90.54(9)	N(7b)−Fe(2)−O(2b)	89.35(10)
O(1a)−Fe(1)−O(2a)	56.05(9)	O(1b)−Fe(2)−O(2b)	57.88(8)

solids, pale yellow for Fe(TIM)(HCO_2)$_2$ (**4**) and light green for Fe(TIM)(CH_3CO_2)$_2$ (**5**). However, we were unsuccessful in growing crystals large enough to carry out an X-ray structural study of **4** and **5**. On the other hand, reaction of TIM with ferrous perchlorate resulted in the immediate appearance of an intense purple-red coloration of the reaction mixture. The intensely colored compound formed in the absence of coordinating anion, probably a low-spin $Fe^{II}N_6$ species, was very soluble and could not be precipitated out of the solution. Subsequent methatheses reactions carried out with different alkaline carboxylates yielded new species which slowly precipitated out of the reaction medium as faintly colored microcrystalline solids, white-pale pink for **1**, white-light green for **2**, and brown-orange for **3**. Elemental anlyses indicated the simultaneous presence of one carboxylate and one perchlorate anions for **1** and **2** and half an oxalate and one perchlorate anions for **3**, allowing in conjunction with IR spectroscopy (see below) to formulate these new species as Fe(TIM)($C_6H_5CH_2CO_2$)](ClO_4) (**1**), [Fe(TIM)(CH_3CO_2)](ClO_4) (**2**), and Fe_2(TIM)$_2$(C_2O_4)(ClO_4)$_2$ (**3**). While we succeeded to subsequently grow crystals of **1** and **2**, we were unsuccessful in growing large enough crystals to carry out an X-ray structural study of **3**.

Molecular Structure of 1 and 2. The molecular structure of [Fe(TIM)($C_6H_5CH_2CO_2$)](ClO_4) (**1**) consists of a [Fe(TIM)($C_6H_5CH_2CO_2$)]$^+$ complex cation, shown in Figure 2, and a perchlorate counteranion.

The iron(II) is hexacoordinated to N1, N2, N3, and N4 from the TIM ligand (2.102−2.176 Å) and O1 and O2 from the phenylacetate anion. The bidentate coordination mode of the phenylacetate anion (Fe−O1 = 2.164(2) Å, Fe−O2 = 2.328(2) Å and O1−Fe−O2 = 57.9°) is significantly asymmetric and results from the steric constraint imposed by the three methylene bridges between the imidazole rings of TIM which does not allow an equatorial tetradentate coordination mode; i.e., tetracoordination through N1, N2, N3, and N4 is not compatible with a planar conformation of TIM. As a result, Fe is 0.6637(2) Å above the average N1, N2, N3, N4 plane and the symmetry of the N_4O_2 donor set

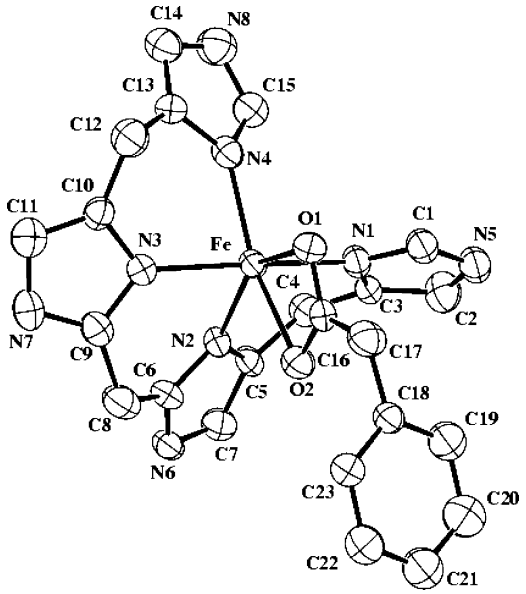

Figure 2. ORTEP view of the [Fe(TIM)($C_6H_5CH_2CO_2$)](ClO_4) (**1**) complex with atom numbering.

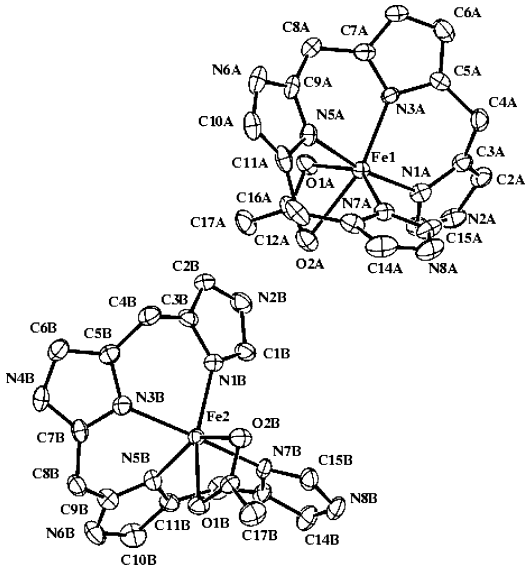

Figure 3. ORTEP view of the [Fe(TIM)(CH_3CO_2)](ClO_4) (**2**) complex with atom numbering.

to Fe^{II} is severely distorted from the octahedral one (see bond lengths and angles in Table 2 and see Figure 2).

Adjacent complex cations are hydrogen-bonded together through NH(5a)···O1 ($-1/2 + x$, $1 - y$, z) and NH(7a)···O2 ($-1/2 + x$, $1/2 + y$, $1/2 + z$) imidazole−carboxylate contacts and also to perchlorate counteranions through NH(6a)···O3 ($1/2 + x$, $1 - y$, z), NH(8a)···O42 ($1/2 + x$, $1/2 + y$, $-1/2 + z$) and NH(8)···O51 ($1/2 + x$, $1/2 + y$, $-1/2 + z$) imidazole−perchlorate contacts ($2.79 < N\cdots O < 3.20$ Å, CIF file) yielding a dense 3D network responsible for the crystal packing.

The molecular structure of [Fe(TIM)(CH_3CO_2)](ClO_4) (**2**) consists of two slightly different [Fe(TIM)(CH_3CO_2)]$^+$ complex cations, shown in Figure 3, and perchlorate counteranions, both termed a and b.

The overall structure of the a and b complex cations of **2**, [Fe(TIM)(CH_3CO_2)]$^{2+}$, is virtually the same as in complex

Table 4. Carboxylate Anions: IR Data (cm^{-1}) for Complexes **1**−**5** ($\Delta = \nu_{as}(CO_2^-), \nu_s(CO_2^-)$) and for the Corresponding Sodium Carboxylate (Δ_{ionic})

no.	complex	$\nu_{as}(CO_2^-), \nu_s(CO_2^-)$	D	Δ_{ionic}
1	$[Fe^{II}(TIM)(C_6H_5CH_2CO_2)](ClO_4)$	1557, 1405	152	190
2	$[Fe^{II}(TIM)(CH_3CO_2)](ClO_4)\cdot MeOH$	1575, 1475	100	165
		1575, 1425	150	
3	$(Fe^{II})_2(C_2O_4)(TIM)_2(ClO_4)_2$	1639, 1315	324	320
4	$Fe^{II}(TIM)(HCO_2)_2$	1595, 1341	254	240
5	$Fe^{II}(TIM)(CH_3CO_2)_2\cdot MeOH$	1574, 1420	154	165
		1574, 1400	174	

1, with $Fe^{II}a$ and $Fe^{II}b$ ions hexacoordinated to N1, N3, N5, and N7 from the TIM ligands (2.112−2.217 Å; see Table 3 for details) and O1 and O2 from bidentate acetate anions. The most striking difference between the a and b complex cations of **2** results from the variation in bidentate carboxylate coordination mode: while the bidentate coordination of the acetate is almost symmetrical in site b (Fe2−O1b = 2.227(2) Å, Fe2−O2b = 2.263(2) Å, and O1b−Fe2−O2b = 57.9°), it is even more asymmetrical in site a (Fe1−O1a = 2.108(2) Å, Fe1−O2a = 2.435(3) Å, and O1a−Fe1−O2a = 56.1°) than in complex **1**. As in complex **1**, the steric constraint imposed by the three methylene bridges between the imidazole rings does not allow an equatorial tetradentate coordination mode of the TIM ligand, and consequently, the symmetry of the N_4O_2 donor set to Fe^{II} is severely distorted from the octahedral one (see bond lengths and angles in Table 3 and see Figure 3).

Adjacent complex cations are unevenly hydrogen-bonded together through two NHa···Ob, one NHa···Oa, and one NHb···Oa imidazole−carboxylate contacts and also to perchlorate counteranions through two NHa···Ob, one NHa···Oa, three NHb···Ob, and one NHb···Oa imidazole−perchlorate contacts (2.70 < N···O < 3.20 Å, CIF file) yielding an intricate and dense 3D network between a and b sites, responsible for the crystal packing.

IR Spectroscopy. The asymmetric and symmetric CO_2^- absorptions ($\nu_{as}(CO_2^-)$ and $\nu_s(CO_2^-)$, respectively) observed for the carboxylates in complexes **1**−**5** are summarized in Table 4, together with their difference Δ ($=(\nu_{as}(CO_2^-) - \nu_s(CO_2^-))$ and the usually reported Δ_{ionic} ($=\nu_{as}(CO_2^-) - \nu_s(CO_2^-)$ for the corresponding free carboxylate).

In agreement with the structural determination, the $\nu_{as}(CO_2^-)$, $\nu_s(CO_2^-)$, and Δ values obtained for complex **2**, $[Fe(TIM)(CH_3CO_2)](ClO_4)$, clearly indicate the presence of two different bidentate acetate anions, the coordination mode of one of them being less symmetrical ($\Delta = 150\ cm^{-1}$), and thus closer to a monodentate mode, than that of the other one ($\Delta = 100\ cm^{-1}$).[23,24] It is then very likely that the $\Delta = 150\ cm^{-1}$ value corresponds to the acetate anion of site a, while the $\Delta = 100\ cm^{-1}$ value is attributable to the acetate anion of site b. The Δ values obtained for the acetate anions of complex **5**, $Fe(TIM)(CH_3CO_2)_2$, suggest that while one acetate would not be coordinated to the iron ($\Delta = 175\ cm^{-1}$) the other one would be coordinated in a bidentate mode ($\Delta = 155\ cm^{-1}$), probably with significant asymmetry as in site a of complex **2**.

(23) Deacon, G. B.; Phillips, R. J. *Coord. Chem. Rev.* **1980**, *33*, 227.
(24) Costes, J.-P.; Dahan, F.; Laurent, J.-P. *Inorg. Chem.* **1985**, *24*, 1018.

Table 5. Effective Magnetic Moment (μ_{Eff}/Fe) at Selected Temperatures for Complexes **1**−**5**

complex (no.)	temp, K				
	300	100	30	11	2
$[Fe(TIM)(C_6H_5CH_2CO_2)](ClO_4)$ (**1**)	5.15	5.20	5.15	4.83	4.40[a]
$[Fe(TIM)CH_3CO_2](ClO_4)\cdot MeOH$ (**2**)	5.41	5.38	5.27	4.95	3.43
$Fe_2(TIM)_2(C_2O_4)(ClO_4)$ (**3**)	4.68	4.52	3.87	2.38	1.29
$Fe(TIM)(HCO_2)_2$ (**4**)	5.30	5.18	4.87	4.13	2.24
$Fe(TIM)(CH_3CO_2)_2\cdot MeOH$ (**5**)	5.10	5.12	5.05	4.78	3.58

[a] $T = 5$ K.

The coordination modes of the phenylacetate in **1**, oxalate in **3**, and formate in **4**, may be tentatively assessed by comparison with the Δ value of the corresponding ionic carboxylate in a way similar to that suggested by Deacon and Phillips.[23] Compared to the $\Delta = 190\ cm^{-1}$ value for the ionic form, the $\Delta = 150\ cm^{-1}$ value obtained for the phenylacetate in complex **1** suggests a bidentate coordination mode, in agreement with the molecular structure of **1**. The $\Delta = 325\ cm^{-1}$ value obtained for the oxalate in complex **3** is close to that reported for the side-on η^2 bridging bis-bidentate coordination mode of the oxalate dianion.[25] The unique $\Delta = 255\ cm^{-1}$ value obtained for the formate in complex **4** is higher than the $\Delta = 240\ cm^{-1}$ value reported for the ionic formate, suggesting that both formate anions of **4** may be monodentate.

The 660, 750, and 1155 cm^{-1} absorptions may be attributed to the Γ and Δ ring deformations and Δ imidazole ring breathing vibrations of TIM, respectively.

Magnetic Susceptibility. The magnetic susceptibility data for complexes **1**−**5** were collected in the 2−300 K temperature range, and μ_{eff}/Fe values for selected temperatures are reported in Table 5.

The effective magnetic moment/iron at 300 K (5.10−5.41 μ_B) is larger than the $S = 2$ spin-only value of 4.9 μ_B for **1**, **2**, **4**, and **5**, as usually observed for high-spin iron(II) complexes.[11g,26] Although values in excess of 5.2 μ_B at room temperature may indicate the presence of impurities, the Mössbauer spectra (see below) did not show the presence of ferric contaminant, as also confirmed by EPR spectroscopy. The temperature dependence of the magnetic moments below 30 K indicates operation of zero-field splitting of the high-spin iron(II) ground state.The μ_{eff}/Fe values for complexes **1**, **2**, and **5** are practically constant, in the 300−30 K range, in agreement with the mononuclear high-spin iron(II) nature of these complexes, as confirmed by the single-crystal X-ray study of **1** and **2**.

We have analyzed the variation of the magnetic susceptibility of $Fe(TIM)(HCO_2)_2$ (**4**) by employing the expression derived from the isotropic spin-exchange Hamiltonian $H = -2JS_1S_2$ ($S_1 = S_2 = 2$) and the van Vleck equation[27] modified

(25) (a) Lloret, F.; Julve, M.; Mollar, M.; Castro, I.; LaTorre, J.; Faus, J.; Solans, X.; Morgenstern-Badarau, I. *J. Chem. Soc., Dalton Trans.* **1989**, 729. (b) Lloret, F.; Julve, M.; Mollar, J.; Faus, J.; Solans, X.; Journaux, Y.; Morgenstern-Badarau, I. *Inorg. Chem.* **1990**, *29*, 2232. (c) Armentano, D.; De Munno, G.; Lloret, F.; Palii, A. V.; Julve, M. *Inorg. Chem.* **2002**, *41*, 2007.
(26) (a) Kennnedy, B. J.; Murray, K. S. *Inorg. Chem.* **1985**, *24*, 1552. (b) Mabad, B.; Cassoux, P.; Tuchagues, J.-P.; Hendrickson, D. N. *Inorg. Chem.* **1986**, *25*, 1420.
(27) O'Connor, C. J. *Prog. Inorg. Chem.* **1982**, *29*, 203.

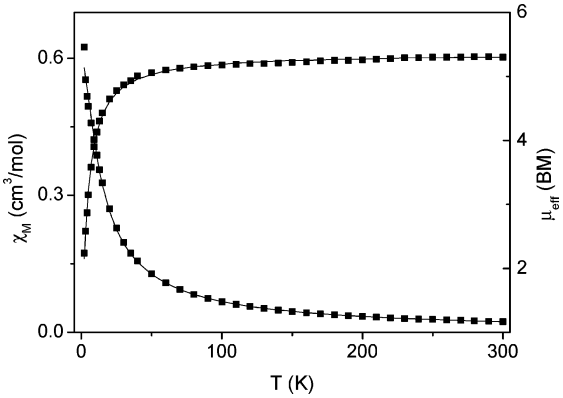

Figure 4. Variable-temperature magnetic susceptibility data for Fe(TIM)-$(HCO_2)_2$ (**4**). The solid lines result from a least-squares fit of the data with the model described in the text.

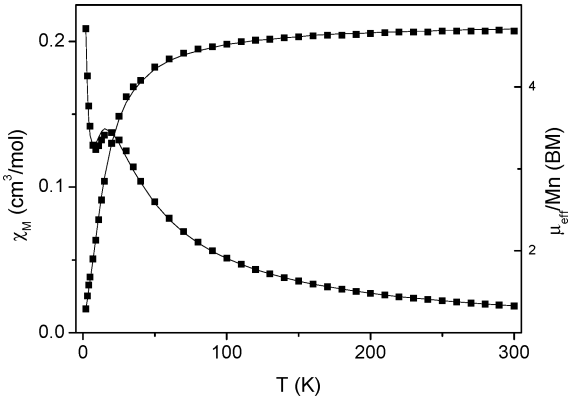

Figure 5. Variable-temperature magnetic susceptibility data for $Fe_2(TIM)_2$-$(C_2O_4)(ClO_4)$ (**3**). The solid lines result from a least-squares fit of the data with the model described in the text.

to take into account intermolecular interactions in the molecular field approximation (zj' with z = number of nearest neighbors and j' = coupling constant between nearest neighbors).[28] The least-squares refinement calculated from this model yielded a reasonable fit (Figure 4) for the parameters $J = -0.5$ cm^{-1}, $zj' = -1$ cm^{-1}, $g = 2.17$, and Par = 2.5% (Par accounts for a $S = 2$ paramagnetic impurity). Attempts to fit the experimental data with the theoretical magnetic susceptibility calculated by exact diagonalization of the effective spin Hamiltonian taking into account single-ion zero-field splitting (ZFS)[29] did not improve the quality of the fit. The minute value of the isotropic interaction J and the larger value of the zj' intermolecular interactions parameter, together with the likeliness of a nonbridging monodentate coordination mode of the formate anions indicated by IR spectroscopy, suggest that intermolecular interactions are predominant, if not exclusive, in complex **4**.

The overall magnetic behavior of complex **3** clearly indicates weak antiferromagnetic interactions between the iron(II) centers, and the iron/TIM/oxalate/ClO_4 ratios and IR spectroscopy suggests the side-on η^2 bis-bridging bidentate coordination mode of the oxalate dianion, i.e., oxalate-bridged dinuclear iron(II) species. Analysis of the thermal variation of the magnetic susceptibility of **3** by employing the expression derived from the isotropic spin-exchange Hamiltonian $H = -2JS_1S_2$ ($S_1 = S_2 = 2$) and the van Vleck equation modified to take into account intermolecular interactions in the molecular field approximation did not yield an acceptable fit. On the other hand, fitting the experimental data with the theoretical magnetic susceptibility calculated by exact diagonalization of the effective spin Hamiltonian taking into account single-ion zero-field splitting (ZFS)[29] dramatically improved the quality of the fit for the parameters $J = -2.1$ cm^{-1}, $D = -3.35$ cm^{-1}, $g = 1.92$, and Par = 7.2% (Figure 5). The relatively high percentage of $S = 2$ paramagnetic impurity, resulting from the presence of a small amount of mononuclear Fe(TIM)(C_2O_4Na)(ClO_4) species (see Experimental Section), may hinder an accurate simultaneous evaluation of J, D, and g and lead to the low calculated g value (1.92).

Mössbauer Spectroscopy. The Mössbauer spectra of complexes **1** and **3**−**5** recorded in the 4−293 K temperature range consist of a single quadrupole-split doublet. The spectra of **2** consist of two quadrupole-split doublets. All spectra were least-squares-fitted with Lorentzian lines, and the resulting isomer shift (δ) and quadrupole splitting (ΔE_Q) parameters for selected temperatures are listed in Table 6. The δ and ΔE_Q values clearly indicate the presence of high-spin Fe^{II} in all complexes. The δ values are weakly temperature dependent due to second-order Doppler shift.[30]

The 1.11−1.16 mm·s^{-1} isomer shift values obtained for complexes **1**−**5** at 80 K are in the lower part of the δ range observed for a [FeN_4O_2] core,[11d−g] likely as a result of the charge delocalization at the bidentate carboxylate and π interaction with the metal center.

The quadrupole splitting values may be divided into three groups: the formate complex (**4**) is characterized by the larger ΔE_Q values, one of the sites of complex **2** is characterized by the smaller ΔE_Q values, and complexes **1**, **3**, and **5** and the remaining site of complex **2** are characterized by intermediate ΔE_Q values. The large ΔE_Q value observed for complex **4** at 4 K (4.02 mm·s^{-1}) is characteristic of an orbital singlet ground state, and its weak temperature dependence (3.64 mm·s^{-1} at 293 K) indicates that the energy separation between the ground and higher orbital states is quite large, i.e., that the crystal field distortion of the octahedral symmetry has a strong axial term.[31] This result agrees with a monodentate coordination of both formate anions as suggested from IR spectroscopy: indeed this coordination mode may easily allow an axially distorted N_4O_2 octahedral ligand environment. The 3.06 mm·s^{-1} ΔE_Q value observed for complex **1** at 4 K is large enough to indicate an orbital singlet ground state, and its weak temperature dependence (2.54 mm·s^{-1} at 293 K) indicates that the crystal field distortion of the octahedral symmetry is dominated by an axial term.[31] This result agrees with the structural parameters indicating a distorted octahedral coordination

(28) Ginsberg, A. P.; Lines, E. P. *Inorg. Chem.* **1972**, *11*, 2289.
(29) Garge, P.; Chikate, R.; Padhye, S.; Savariault, J.-M.; de Loth, P.; Tuchagues, J.-P. *Inorg. Chem.* **1990**, *29*, 3315.
(30) Greenwood, N. N.; Gibbs, T. C. *Mössbauer Spectroscopy*; Chapman and Hall: New York, 1971.
(31) Sams, J. R.; Tsin, T. B. *Inorg. Chem.* **1975**, *14*, 1573.

Table 6. Representative Least-Squares-Fitted Mössbauer Data (Isomer Shift, δ, Referenced to Metallic Iron at Room Temperature, Quadrupole Splitting, ΔE_Q, and Width at Half-Height, $\Gamma/2$) for Complexes **1**−**5**

complex (no.)	T, K	δ, mm·s^{-1}	ΔE_Q, mm·s^{-1}	$\Gamma/2$, mm·s^{-1}	area ratio, %
[Fe(TIM)($C_6H_5CH_2CO_2$)](ClO_4) (**1**)	293	1.006(2)	2.536(2)	0.115(2)	100
	80	1.111(1)	3.080(2)	0.131(1)	100
	4	1.128(1)	3.059(1)	0.135(1)	100
[Fe(TIM)CH_3CO_2](ClO_4)·MeOH (**2a**)	293	1.006(4)	2.816(9)	0.123(7)	46(3)
	80	1.119(3)	3.261(5)	0.123(4)	51(1)
	4	1.134(2)	3.291(3)	0.138(3)	49(1)
[Fe(TIM)CH_3CO_2](ClO_4)·MeOH (**2b**)	293	1.015(4)	2.130(8)	0.133(7)	54(3)
	80	1.139(2)	2.124(5)	0.126(4)	49(1)
	4	1.158(1)	2.232(5)	0.179(4)	51(1)
Fe_2(TIM)$_2$(C_2O_4)(ClO_4) (**3**)	293	1.039(1)	2.713(7)	0.131(6)	100
	80	1.147(2)	3.265(4)	0.141(3)	100
	4	1.195(2)	3.131(3)	0.167(2)	100
Fe(TIM)(HCO_2)$_2$ (**4**)	293	1.042(1)	3.636(2)	0.127(2)	100
	80	1.165(1)	4.110(1)	0.135(1)	100
	4	1.177(1)	4.023(2)	0.147(2)	100
Fe(TIM)(CH_3CO_2)$_2$·MeOH (**5**)	293	0.987(1)	2.825(2)	0.154(2)	100
	80	1.104(2)	3.252(3)	0.184(3)	100
	4	1.112(3)	3.55(2)	0.16(1)	36(6)
	4	1.126(2)	3.18(2)	0.186(6)	64(6)

sphere as a result of the asymmetric bidentate coordination mode of the phenylacetate: while five M−L bonds are in the 2.102−2.176 Å range, the Fe−O2 bond is much longer (2.326 Å). The structure of complex **2**, site a, evidences an even more asymmetric bidentate coordination mode of the acetate with five M−L bonds in the 2.108−2.166 Å range while the Fe1−O2a bond length equals 2.435 Å. Among the two iron(II) sites distinguished by Mössbauer spectroscopy the one characterized by the larger ΔE_Q value at 4 K (3.29 mm·s^{-1}) and a weak temperature dependence (2.82 mm·s^{-1} at 293 K) may be unambiguously assigned to site a by comparison of the ΔE_Q values of **1**, and **2a**,**b**: indeed, while the ΔE_Q values of **1** and **2a** compare favorably, the ΔE_Q values of **2b** (2.23 and 2.13 mm·s^{-1} at 4 and 293 K, respectively) clearly indicate a very different site symmetry at the iron center. It is worth noting that IR spectroscopy indicates very similar $\Delta = \nu_{as}(CO_2^-) - \nu_s(CO_2^-)$ values (150 cm^{-1}) for the asymmetric bidentate coordination modes of the phenylacetate in **1** and of the acetate in site a of complex **2**, compared to the much lower $\Delta = 100$ cm^{-1} value for the symmetrical bidentate coordination mode of the acetate in site b. The fact that both spectroscopies strongly sense the difference between these symmetrical and asymmetrical bidentate coordination modes of carboxylates clearly indicates the importance of both the structural and electronic effects of this apparently tenuous carboxylate shift.[32] The large ΔE_Q values of complexes **3** and **5**, 3.13 and 3.55 mm·s^{-1} at 4 K, respectively, also indicate an orbital singlet ground state, and their weak temperature dependence (Table 6) indicates that the crystal field distortion of the octahedral symmetry is also dominated by an axial term.[31] Considering the closeness of the ΔE_Q parameters of complexes **3** and **5** to those obtained for **1** and **2a**, an asymmetric bidentate coordination mode of the oxalate in **3** and of one of the acetate anions in **5** (see IR section) may be inferred.

(32) Rardin, R. L.; Tolman, W. B.; Lippard, S. J. *New J. Chem.* **1991**, *15*, 417.

Discussion

Versatility of the $Fe^{II}N_4O_2$ Coordination Geometry as a Result of the Steric Demand of the Tetraimidazole Ligand, TIM, and the Flexibility of the Carboxylate Coordination. The TIM ligand has been selected for preparing the present series of complexes because the steric demand imposed by the three methylene bridges requires coordination through the four imidazole nitrogen donors of TIM with a geometry intermediate between planar equatorial and folded conformations. The FeN_4 set of atoms forms an umbrella where the iron is 0.6637(2) Å above the four nitrogen donors: coordination at the apical position below the umbrella is thus at serious disadvantage. On the other hand, the space needed for bidentate coordination of a carboxylate, although larger than for the monodentate one, is smaller than the space available around two cis positions of a regular octahedron. It was thus expected that involvement of TIM as a tetradentate ligand in the coordination sphere of iron would favor the bidentate coordination of a carboxylate, above the FeN_4 umbrella, as actually shown by the molecular structure of complexes **1** and **2**. Indeed, both structure clearly show that while there is not enough room to accommodate monodentate coordination of acetate or phenylacetate anions below the FeN_4 umbrella, the space available above the umbrella is large enough to accommodate bidentate coordination of these carboxylates. Although the crystal structures of complexes **3**−**5** could not be obtained, the composition, IR, and Mössbauer data converge on structural hypotheses consistent with the rationale above. In complex **3**, FeN_4 umbrellas are most probably twinned through bis-bidentate oxalate bridges. In complex **5**, the acetate anion is too bulky to coordinate in a monodentate mode at the apical position below the FeN_4 umbrella. Then, while one acetate anion is coordinated in a bidentate mode above the FeN_4 umbrella, the second one is not coordinated. In complex **4**, the less bulky formate anions coordinate in a monodentate mode at the apical positions below and above the FeN_4 umbrella.

Another point of interest is the diversity in bidentate coordination modes of carboxylates evidenced by the molecular structure of complexes **1** and **2**. While the bidentate coordination mode of the acetate anion is strongly asymmetrical in site a and symmetrical in site b of complex **2**, the bidentate coordination mode of the phenylacetate anion is asymmetrical in complex **1**, although less than in site a of complex **2**. The origin of this diversity in carboxylate bidentate coordination modes probably lies in the quite strong and numerous but different hydrogen bonds in which these carboxylates are involved with the $NH_{imidazole}$ functions of adjacent molecules, to yield the 3D crystal packings of **1** and **2**. As mentioned earlier, this diversity in carboxylate bidentate coordination modes has allowed us to clearly show the importance of both the structural and electronic effects of this apparently tenuous carboxylate shift through both IR and Mössbauer spectroscopy. This result further illustrates possible intermediate states in the carboxylate shift and supports the conclusions drawn by Lippard et al. about the likeliness of a prominent role of the carboxylate shift in biological systems.[32]

As previously underlined by Nordlund et al.,[33] for the Fe1 site of the iron center in the *E. coli* ribonucleotide reductase B2 protein, the bidentate coordination mode of the carboxylate endows the metal center with both trigonal bipyramidal and octahedral features. The differences in bidentate coordination modes of carboxylates evidenced by the molecular structure of complexes **1** and **2** deserve an additional comment with regard to the resulting versatility in symmetry of the iron coordination sphere. Due to the small O1−Fe−O2 angle (56−58°) and $[O\cdots C\cdots O]^-$ delocalization, the bidentate coordination mode of the carboxylate may be regarded as intermediary between one and two Fe−O bonds, resulting in a coordination formally intermediary between $[FeN_4O]$ and $[FeN_4O_2]$. While this picture is satisfactory for a symmetrical bidentate coordination, it is as less accurate as the bidentate coordination mode is more asymmetrical: the picture is then closer to distorted octahedral than intermediary between penta- and hexacoordinated. In the case of complexes **1** and **2**, we then expect site **2a** (Fe1−O1a = 2.108, Fe1−O2a = 2.435 Å) to be better described as distorted octahedral, site **2b** (Fe2−O1b = 2.227, Fe2−O2b = 2.263 Å) to be better described as intermediary between penta- and hexacoordinated, and complex **1** (Fe−O1 = 2.164, Fe−O2 = 2.328 Å) to be intermediary between sites **2a** and **2b**. As previously noted (Mössbauer section), the differences in symmetry of the iron coordination sphere associated with the differences in symmetry of the bidentate coordination mode of the carboxylate (to the exclusion of TIM, the tetradentate coordination of which is formally identical in **1** and **2a**,**b**) is dramatically reflected in the values of the quadrupole splitting parameter (Table 6).

Comparison with the Non-Heme Ferrous Site of Photosynthetic Systems. The noteworthy observations resulting from a structural comparison of the iron ligand environment in complexes **1** and **2** to the non-heme ferrous site of photosynthetic systems may be summarized as follows: (i) In both types of systems, synthetic and biological, the ligand environment to the ferrous iron includes four $N_{imidazole}$ and the two O donor atoms of a bidentate carboxylate. (ii) Among complex **1** and sites **2a**,**b**, the metric parameters of site **2b** including the symmetrically chelated bidentate carboxylate are closer to those in the non-heme ferrous site of *Rhodopseudomonas viridis*[9] and *R. sphaeroides*.[10] The superimposed drawings of the iron coordination environment in site **2b** and in the non-heme ferrous site of *R. viridis* shown in Figure 6 illustrate the quality of the structural modeling attained.

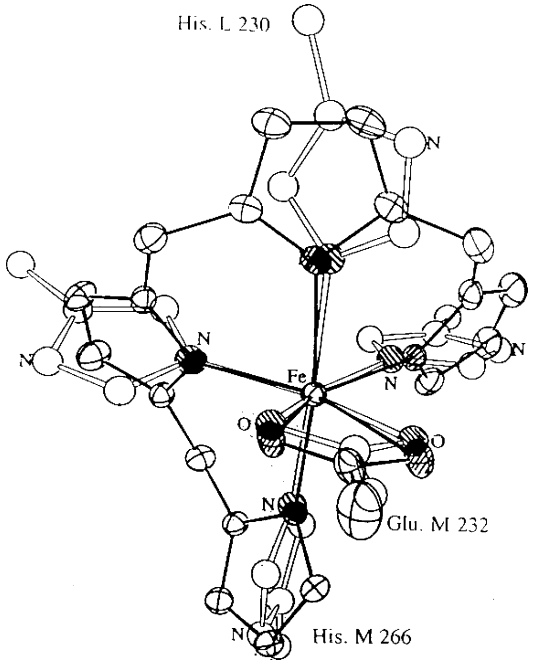

Figure 6. Superimposed ORTEP plots of the iron coordination environment in site b of $[Fe(TIM)(CH_3CO_2)](ClO_4)$ (**2**) and in the non-heme ferrous site of *Rhodopseudomonas viridis*.

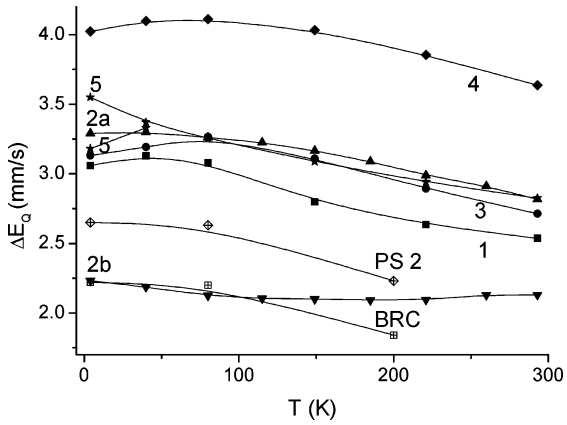

Figure 7. Compared temperature-dependence of the quadrupole splitting for complexes **1**−**5**, PS 2 particles, and bacterial reaction centers. The lines drawn between the experimental values are intended to connect the values corresponding to a given iron site and do not represent calculated values.

In Figure 7, the temperature dependence of the quadrupole splitting of complexes **1**−**5** is compared to that of the non-heme ferrous site in *R. sphaeroides* reaction centers[34] and of photosystem 2 (PS 2) particles from *Chlamydomonas reinhardtii*.[35] In the bacterial reaction centers, the iron is in

(33) Nordlund, P.; Sjöberg, B. M.; Eklund, H. *Nature* **1990**, *345*, 593.

a highly distorted octahedral ligand environment, as depicted in Figure 6.

On the basis of spectroscopic evidence and sequence homologies with the structurally characterized photosynthetic bacteria,[9,10] the non-heme ferrous center of PS 2 is also believed to have the four imidazole ligands, but the identity of the remaining ligand(s) differ for bacteria and PS 2: in PS 2, at least one of the remaining coordination sites is occupied by bicarbonate, most likely in the bidentate mode.[35,36] Interestingly enough, the quadrupole splittings of complexes **1**−**3** and **5**, which include four $N_{imidazole}$ and the two O donor atoms of a bidentate carboxylate, are close enough to those of the non-heme ferrous site of photosynthetic systems but significantly different from those of complex **4** in which the monodentate coordination of the caxboxylates yields an axially distorted octahedral symmetry. In complete agreement with the result of the structural comparison reported in the previous section, site **2b** including the symmetrically chelated bidentate carboxylate (strongly distorted ligand environment better described as intermediary between penta- and hexacoordinated) has the quadrupole splitting values closest to those of the non-heme ferrous site of *R. sphaeroides*.[34] Site **2a**, which includes the more asymmetrically chelated bidentate carboxylate, resulting in an axially distorted octahedral ligand environment, is characterized by quadrupole splitting values higher than those of the non-heme ferrous site of photosynthetic systems. Complex **1**, which includes a bidentate carboxylate less asymmetrically chelated than site **2a**, is characterized by quadrupole splitting values closer to those of the non-heme ferrous center of PS 2 (although slightly higher). From this comparison of the quadrupole splittings, it may be suggested that the ligand environment of the non-heme ferrous center of PS 2 is close to the axially distorted octahedral symmetry resulting from an asymmetrical bidentate coordination of the $-CO_2$ motif.

Acknowledgment. We are grateful to CNRS and European Community (TMR Contract FMRX-CT980174) for financial support and to J.-C. Chottard for stimulating discussions.

Supporting Information Available: X-ray crystallographic data in CIF format for the structures of complexes **1** and **2**. This material is available free of charge via the Internet at http://pubs.acs.org.

IC034907K

(34) Boso, B.; Debrunner, P.; Okamura, M. Y.; Feher, G. *Biochim. Biophys. Acta* **1981**, *638*, 173.
(35) (a) Petrouleas, V.; Diner, B. A. *Biochim. Biophys. Acta* **1990**, *1015*, 131. (b) Diner, B. A.; Petrouleas, V. *Biochim. Biophys. Acta* **1990**, *1015*, 141.
(36) Hienerwadel, R.; Berthomieu, C. *Biochemistry* **1995**, *34*, 16288.